REVIEW ARTICLE
https://doi.org/10.1038/s41560-018-0295-9

nature energy

Characterization and performance evaluation of lithium-ion battery separators

Marie Francine Lagadec, Raphael Zahn and Vanessa Wood*

Lithium-ion batteries (LIBs) with liquid electrolytes and microporous polyolefin separator membranes are ubiquitous. Though not necessarily an active component in a cell, the separator plays a key role in ion transport and influences rate performance, cell life and safety. As our understanding of separator properties and the interactions between the separator and the electrolyte deepens, it becomes evident that there are opportunities for improving separators to help meet the greater demands that new applications place on LIB technology. Here, we review the impact of the separator structure and chemistry on LIB performance, assess characterization techniques relevant for understanding structure–performance relationships in separator membranes, and provide an outlook on next-generation separator technology. Insights from this Review indicate that LIB performance can be improved by taking into account the interplay of the separator with its surroundings and indicate that, in the future, separators will be designed to play a more active role in LIB operation. Current and emerging characterization techniques will play an important role in guiding this evolution in separator technology.

Today's commercial rechargeable lithium-ion batteries (LIBs) consist of two porous electrodes laminated on metallic current collectors and electronically isolated by porous polymeric membranes. The pore space of the separator and electrode is infilled with liquid electrolyte (Fig. 1a). The electrolyte-filled pore space of the separator membranes allows transfer of lithium ions from the negative porous electrode (anode) to the positive porous electrode (cathode) during discharge and back again during charge, while preventing short circuits between the positive and negative electrodes.

Most commercially available LIB separators are polyolefin membranes made from either semi-crystalline polyethylene (PE) and/or polypropylene (PP). They are typically less than 25 µm thick and have complex three-dimensional structures (Fig. 1b,c) commonly with a porosity, ε, of around 40% (Table 1).

Separators are not active components in batteries, but they influence cell cost, life, performance and safety[1]. Early reviews on separators focused on characterization methods for separator properties that are of particular importance during cell manufacturing (for example, tensile strength, Gurley value, electrolyte uptake) and for cell safety[2]. More recent reviews[3,4] have summarized current manufacturing techniques for polyolefin separators and the resulting separator microstructures, and examined how separators influence LIB performance with respect to ionic conductivity, electrolyte uptake, and thermomechanical and electrochemical stability. Another review[5] has addressed in detail recent improvements to LIB separator performance enabled by various surface modifications.

In this Review, we describe how the structure and the chemistry of microporous polymer separators as well as their interaction with liquid electrolytes affect LIB performance, and the experimental methods and simulation approaches to assess separator structure and function. To do so, we take the following approach. First, we explain the importance of high ionic conductivity and homogeneous ionic transport through a separator. Second, we describe the separator properties that have the greatest impact on the ionic conductivity and the homogeneity of transport. Third, we survey how these separator properties can be characterized. Finally, we consider what this know-how implies for next-generation separator technology.

This Review adds to the existing literature on separator technology in two ways. First, we emphasize that a separator is not a passive component and detail how the interactions between the separator and its environment influence battery performance. Second, this Review assesses the different techniques that have been used to investigate separator performance and that can be used to facilitate the rational design of next-generation separators.

Ionic transport in separators

In this section, we discuss why a well-designed separator should facilitate homogeneous ionic transport through its electrolyte-filled pore network to ensure good LIB performance and minimize degradation[6,7]. We explain the principles of ionic transport and the challenges associated with making transport homogeneous across the separator.

Ionic transport and voltage losses. As the conductivity of ions in an electrolyte, σ_{el}, is finite (that is, there is a resistance associated with moving ions), voltage loss occurs during discharging and additional voltage is needed during charging to drive ionic current. These voltage differences are referred to as the electrolyte resistance overpotential[8]. The lower the ionic conductivity and the larger the current, the larger the electrolyte resistance overpotential. Large overpotentials prevent the theoretical voltage and specific capacity of the cell from being obtained[9], and contribute to degradation due to heat generation[10] and lithium plating[11].

Ionic conductivity is related to the concentration of the salt, c, and its diffusion coefficient in the electrolyte, $\sigma_{el} \propto c \times (D^+ + D^-)$, where D^+ is the diffusion coefficient of Li^+ ions and D^- is the diffusion coefficient of the electrolyte's anions (for example, hexafluorophosphate, PF_6^-). The electrolyte's diffusion coefficients D^+ and D^- are themselves concentration dependent and decrease with increasing salt concentration. Accordingly, σ depends on c and strongly increases for increasing ion concentrations (up to ~1 M for $LiPF_6$-containing electrolytes) before levelling off and decreasing again (Fig. 1d)[12]. Therefore, the magnitude of the overpotential depends on ion concentration, increasing strongly

Department of Information Technology and Electrical Engineering, ETH Zürich, Zürich, Switzerland. *e-mail: vwood@ethz.ch

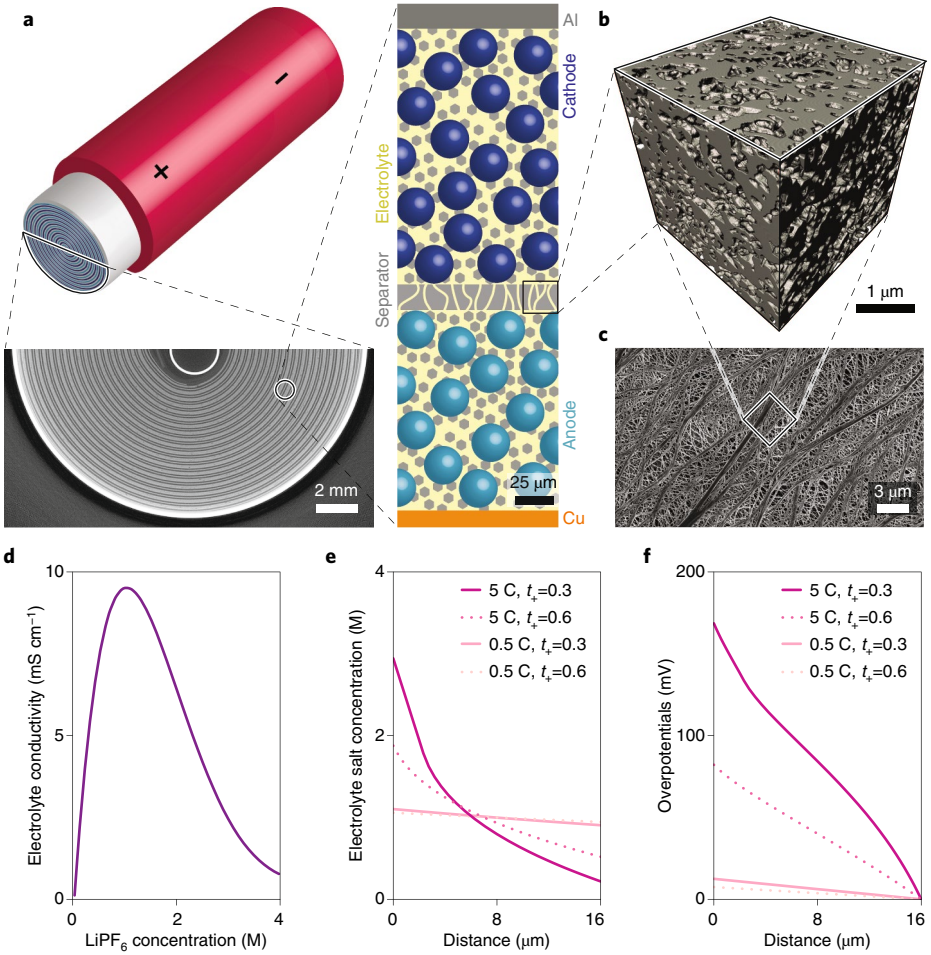

Fig. 1 | Separators in LIBs. a, Schematic and X-ray tomographic image showing the tightly wound layers of anode, separator and cathode of a cylindrical cell and a zoomed-in schematic of the layer structure. **b**, FIB-SEM tomographic rendering of a Targray PE16A separator (raw data behind the rendering are available in ref. [49]). **c**, Top-view SEM image of the same separator. **d**, Electrolyte conductivity as a function of electrolyte salt ($LiPF_6$) concentration in a 1:1 mass-ratio mixture of ethylene carbonate and ethyl methylcarbonate. **e**,**f**, COMSOL simulations of electrolyte salt concentration (**e**) and electrolyte potential (**f**) as function of distance across the separator in a symmetric Li versus Li cell (to exclude effects of electrode structure). Current densities relate to charging rates for a 3 mAh cm^{-2} graphite electrode. Panels adapted from: **a**, ref. [98], Springer Nature Ltd; **c**, ref. [20], ECS.

in the presence of regions of low ($\lesssim$0.5 M) or high ($\gtrsim$2.5 M) ion concentrations[13].

The lithium-ion transference number, t_+ (ref. [14]), is an important parameter related to ion concentration. It describes the fraction of the total ionic current carried by Li^+ ions ($t_+ \propto D^+/\sigma_{el}$) and determines the build-up of ion gradients in the electrolyte (that is, regions of very low and very high ion concentration within one cell). For a solid electrolyte, where only Li^+ ions diffuse, $t_+ = 1$. However, for liquid electrolytes, $t_+ < 1$, with typical Li^+ ion transference numbers in the range of 0.3–0.4 (refs. [12,15,16]). This means that, for a given current rate, a distinct ion gradient will develop and the electrolyte resistance overpotentials will be nonlinear versus current.

In the following section 'Impact of a separator on lithium-ion transport', we explain that the conductivity and transference number of ions in the electrolyte-filled pore space of a separator membrane is determined not only by the electrolyte's properties, but also by the separator's structure and the interaction between electrolyte and separator surface. Standard LIB separator structures reduce the ionic conductivities of the electrolyte in the pore space to approximately 5–20% compared to the value of bulk liquid electrolyte[17]. Furthermore, the electrolyte and the separator surface can alter diffusion coefficients, thereby influencing ionic conductivity and transference number.

COMSOL simulations highlight the impact of ionic conductivity and transference number on cell performance. Figure 1e shows the salt concentration gradients in the electrolyte across a 16-µm-thick separator membrane with 40% porosity and a tortuosity of ~2.6 (yielding an effective transport coefficient $\delta = 0.16$) during slow (0.5 C) and fast (5 C) cycling assuming transference numbers of 0.3 and 0.6. At low cycling rates (0.5 C), there are no significant ion gradients across the separator and the electrolyte overpotentials are small (around 10 mV). At high cycling rates (5 C), ion gradients emerge that are considerably more pronounced for low transference numbers (at $t_+ = 0.3$ the concentrations range from 2.9 to 0.2 M; at $t_+ = 0.6$ from 1.9 to 0.5 M). The corresponding electrolyte resistance overpotentials across the separator are shown in Fig. 1f. For fast cycling (5 C), the overpotentials across the electrolyte in the separator reach 80 mV ($t_+ = 0.6$) and 180 mV ($t_+ = 0.3$). An overpotential of 180 mV represents a loss of ~6% of the cell voltage (assuming a nominal voltage of 3.2 V). While these overpotentials are just a fraction of the total electrolyte resistance overpotential (that is, the electrolyte in the electrode pores also contributes to overpotentials)[8], our COMSOL simulations illustrate that increasing electrolyte conductivity and transference number in separator membranes can improve LIB performance, particularly at high current rates.

Table 1 | Properties of selected commercial separators as specified by manufacturers with measured values in brackets

Separator	Type	Porosity (%)	Thickness (μm)	Average pore diameter (porosimetry) (μm)	Gurley value	
					JIS (s)	ASTM (s)
Celgard						
2400	PP	41 (34 (ref. [54]))	25	0.043 (0.09 (ref. [54]))	620	
3401	PP coated	41 (34 (ref. [54]))	25	0.043 (0.09 (ref. [54]))	620	
2500	PP	55 (42 (ref. [54]))	25	0.064 (0.17 (ref. [54]))	200 (180.1 (ref. [96]))	
3501	PP coated	55	25	0.064	200	
2325	PP/PE/PP	39	25	PP: 0.028	620 (570.0 (ref. [96]))	
2320	PP/PE/PP	39	20	PP: 0.027	530 (569±4 (ref. [53]))	
2340	PP/PE/PP	45	38	PP: 0.035	780	
PP1615	PP	40	16	0.05	340	
K1640	PE	40	16		240	
2730	PE	43	20			20
Targray						
PE16A	PE	40±5	16±2	~0.03	180±50 (250±20 (ref. [45]))	
Solupor						
7P03A	PE	85	50	0.3		10
10P05A	PE	83	60	0.5		3
Entek						
Gold LP	PE	37	~20	-	394	

Ensuring homogeneous transport. In addition to high values for Li^+-ion conductivity and transference number for electrolyte in the separator pore space, it is important for cell cycle life and safety that transport is homogeneous. Homogeneous transport of ions to and from the electrodes through the separator layer lowers the risk of incomplete lithiation and delithiation (that is, decreased capacity) and of local overcharge[18].

A typical 18650 power cell features above 600 cm^2 of separator area[19]. Homogeneous transport means that Li^+-ion concentrations and current densities should be similar across the entire separator area. Analysis of pristine commercial separators shows that their structure is homogeneous at length scales above a few micrometres[20]. While this indicates that separator structure can assumed to be homogeneous, inhomogeneous transport can occur as a result of cell manufacturing or during cell operation[21,22].

For example, one aspect influencing the homogeneity of transport in a separator is wetting. Poor wetting of the separator affects LIB manufacturing, where it can bottleneck production and add substantial cost[23]. In addition, incomplete filling of the pore space can close off transport pathways through the pore network[24], effectively reducing the lithium-ion transport capabilities of the separator in specific regions.

Furthermore, while most separators are electrochemically inactive components, their structure, material properties and surface chemistry are dynamically impacted by mechanical, thermal and electrochemical effects occurring in the cell. These effects influence, often inhomogeneously, how the Li^+ ions travel across the electrolyte-filled pore network. After cell assembly, polyolefin separators can interact with the electrolyte, leading to mechanical softening and swelling[25,26]. While LIBs are assembled under small, uniform compression to improve separator wettability[27,28], cell cycling can subject separators to compressive stresses resulting from the volume expansion of active materials and the electrodes during lithiation[29]. These compressive stresses can deform the separator by several micrometres[30]. While a low melting temperature of a separator can be beneficial for shut-down features[31], poor heat dissipation through the separator can limit the discharge rate[32] or cause thermal damage to the separator[33], resulting in loss of structural integrity of the separator and increasing the risk of a short circuit. During cycling, the solid electrolyte interphase (SEI)[34], active material particles or reaction products[35], or Li-metal deposition[20] can block separator pores or enter the pore volume. Indeed, separator areas in contact with lithium-metal-plated graphitic anodes may exhibit crater-like structures of several micrometres in diameter that are the result of localized heating as well as mechanical and/or chemical interactions[33].

For these reasons, it is important to consider the impact of separators on lithium-ion transport, and how separators can be designed to wet uniformly and to mitigate the impact of local thermal, mechanical and electrochemical degradation on their overall transport properties.

Impact of a separator on lithium-ion transport

In this section, we describe the properties that impact Li^+-ion transport in separators. As shown in Fig. 2, we must consider properties related to separator structure, separator chemistry (that is, material composition) and electrolyte chemistry. Parameters used to describe separator structure can be directly linked to ion transport. However, the most important parameters associated with separator chemistry depend on the interaction of the separator and the electrolyte. Furthermore, both separator chemistry and structure will determine how the separator changes on assembly in a cell and during cell operation. Therefore, we divide our discussion of parameters relevant to ionic transport into the following subsections: (1) separator structure, (2) separator–electrolyte interface interactions and (3) separator structure–chemistry interplay.

Separator structure. Separator structure is often described by common microstructural parameters including porosity, ε (that is, the fraction of pore volume to total, pores-plus-material, volume) and the tortuosity, τ (that is, a dimensionless quantity describing the

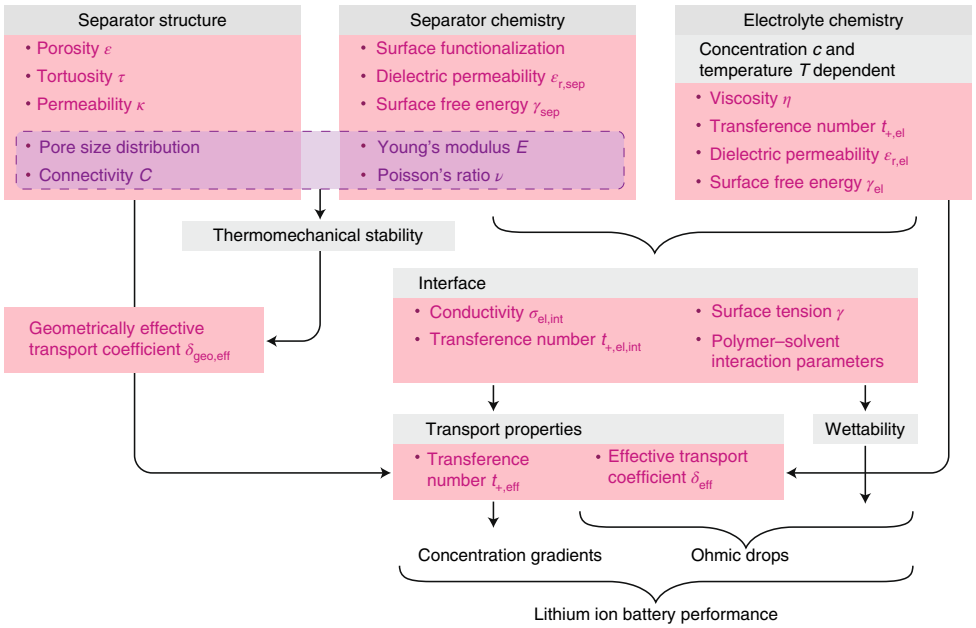

Fig. 2 | Links between properties and performance. Selected separator and electrolyte properties that can be extracted and linked to overall LIB performance under cell operation.

influence of the morphology of the solid phase on the ion flow). While the choice of a liquid electrolyte defines the ionic conductivity, σ_{el}, its effective value is also influenced by separator geometry. Combining information about the amount of pore space (via the porosity, ε) and the influence of the morphology (via the tortuosity, τ), one can determine the effective diffusion, D_{eff} (or effective conductivity σ_{eff}), of Li^+ ions through the separator from $D_{eff} = (\varepsilon/\tau) \times D_{el}$ (or $\sigma_{eff} = (\varepsilon/\tau) \times \sigma_{el}$), where D_{el} and σ_{el} are the diffusion coefficient and conductivity of Li^+ ions in the free electrolyte. The scaling parameter $\delta = \varepsilon/\tau$ is known as the effective transport coefficient. To emphasize that this is a scaling parameter defined by separator geometry, we refer to it as the geometric effective transport, $\delta_{geo,eff}$. With typical values of porosity of 40% and a tortuosity of 2.5, a separator's effective transport coefficient will be around 0.16, meaning that the geometric structure of the separator reduces Li^+-ion transport to 16% of what it would be in a vat of electrolyte, unimpeded by a structure[20].

The permeability, κ, is also used to describe how the geometric structure of the separator constricts Li^+-ion transport. Permeability is related to the electrical resistivity and thus to the effective conductivity[2]. Analogous to Ohm's law describing the flow of electrical current, Darcy's law describes the macroscopic flow of a liquid with viscosity η through a porous sample as:

$$u = -\frac{\kappa}{\eta}\nabla P \quad (1)$$

where u is the average fluid velocity and ∇P is the applied pressure gradient[36]. With dimension m^2, the permeability can be thought of as the effective pore channel area of the dynamically active part of the connected pore space[37]. For separators, the Gurley value, G, which is related to permeability, is generally used instead. The Japanese Industry Standard (JIS) Gurley value is defined as the number of seconds required for 100 cm^3 (100 ml) of air to pass through 1 square inch of a given material at a pressure difference of 4.88 inch of water (that is, 1.21 kPa):

$$G = \frac{\eta_{air} \times V \times L}{\kappa \times \Delta P \times A} \quad (2)$$

where η_{air} is the air viscosity, V is the predefined air volume, L is the membrane thickness, ΔP is the predefined pressure difference and A is the area. Typical values lie between 10^{-17} and 10^{-16} m^2 for the permeability[38] and between 200 and 600 s for the JIS Gurley value (see Table 1). These JIS Gurley values correspond to American Society for Testing and Materials (ASTM) Gurley values (where 10 cm^3 of air and a pressure difference of 12.2 inches of water are used) of ~8 and 25 s.

The tortuosity and permeability values can be defined along specific directions. In a LIB, it is useful to distinguish between transport in the through-plane direction (that is, lithium transport between the two electrodes) and in the two in-plane directions (that is, parallel to the electrodes). While some separators have isotropic properties (for example, biaxially stretched polyethylene), others (for example, uniaxially stretched PP and/or PE) have highly anisotropic parameters[20,39,40].

Recent work has also highlighted the benefit of applying other microstructural descriptors originally defined in topological or network analysis[41] to characterize the performance of separators. Even if separators have very different looking pore structures, they may have identical effective transport coefficients. The connectivity of the pore network, which is related to the Euler–Poincaré characteristic, X, a topological parameter describing a structure's shape, can be helpful in differentiating the performance of such separators. Pore-space connectivity can provide insight into how similar Li^+-ion concentrations will be in neighbouring pores and into the extent to which a local blockage of separator pores near one electrode will lead to a distribution of Li^+-ion concentrations on the other side of the separator[40].

Separator–electrolyte interface interactions. As highlighted in Fig. 2, the chemical composition of the electrolyte (solvent and salt) plays a key role in defining the ionic conductivity and transference number; however, interactions of the solvent and ions with the surface of the separator pores can also impact the conductivity and the transference number. Fundamentally, the ionic conductivity depends on the electrolyte viscosity, η, through the Stoke–Einstein equation that connects the diffusion coefficient, D, of an ion with hydrodynamic radius, r, to the dynamic viscosity, η, of the

electrolyte solution, $D=\frac{k_B T}{6\pi\eta r}$, where k_B is the Boltzmann constant. The electrolyte viscosity, η, is also strongly tied to other physicochemical properties of the electrolyte solution, such as its dielectric permeability, $\varepsilon_{r,el}$, salt concentration, c, or temperature, T (ref. [42]). However, in contrast to the simple concept of effective transport coefficient for describing how separator structure influences transport, no framework exists to explain how the separator's surface properties influence Li^+-ion transport. There are different types of interactions (ionic, polar, hydrophobic, van der Waals) between the molecules in the electrolyte (anions, cations, solvent molecules) and functional groups on the separator's surface. These interactions depend on the degree of dissociation of the electrolyte's salt and the ions' solvation shells. This can lead to local changes in the electrolyte viscosity[43,44] and the diffusion coefficients (D^+ and D^-), thereby modifying the electrolyte's key performance parameters, its conductivity, σ, and its lithium-ion transference number, t_+.

Knowledge of certain parameters, however, can be used to assess the strength of the separator–electrolyte interactions. The surface tension, γ, and the three-phase contact angle determine how well the electrolyte wets the separator. These two parameters depend on the surface free energies of the separator, γ_{sep}, and of the electrolyte, γ_{el}. Solvent compatibility can be analysed with the Hildebrand solubility parameter δ_{HS} (square root of cohesion energy per unit volume; a smaller difference between the δ_{HS} values of the two phases indicates better solvent–polymer compatibility, that is, better polymer wetting by the solvent)[25]. Separator–solvent interactions can also be classified using the Hanson solubility parameters (which distinguishes between the proportion of hydrogen bonding, δ_H, and dispersion plus polar interaction, $\delta_D + \delta_P$, of a phase); a smaller difference between the values of δ_H and (δ_D + δ_P) of the polymer and the solvent also indicates better solvent–polymer compatibility[24]. Finally, the thermodynamic Flory–Huggins interaction parameter, χ, describes the extent to which the polymer chains of the separator and solvent molecules of the electrolyte interact and cause swelling. Furthermore, the extent and type of surface interactions can be influenced by making the separator more hydrophobic or hydrophilic[45].

Interplay between separator structure and chemistry. Although we have described the impact of separator structure and separator–electrolyte interactions as distinct effects, there are complex interdependences between them. For example, the separator structure sets the pore size and the internal surface area, which will determine the extent of the influence of separator–electrolyte interactions (for example, the extent of softening by electrolyte–separator swelling and the effect of microviscosity changes at the surface). Further, as highlighted in Fig. 2, the thermomechanical behaviour of a separator depends not only on the material properties of the separator (for example, Young's modulus, Poisson's ratio), but also on the separator structure. For example, an isotropic structure with small pores will be more susceptible to compressive stresses than an anisotropic structure with large pores in the direction of compression[46].

Characterizing separators

In the following subsections, we describe how to characterize the properties, which are linked to ionic transport as discussed in the section above. We systematically describe methods to quantify (1) separator structure, (2) separator surface–electrolyte interactions and (3) the impact of cell dynamics on separator performance. We summarize these characterization techniques in Table 2, classifying them into imaging and non-imaging (for example, electrochemical and spectroscopic) approaches.

Separator structure. Figure 3 shows surface and cross-sectional scanning electron microscopy (SEM) images for four commercial separators, namely, PE (Fig. 3a), PP (Fig. 3b), ceramic-coated PP (Fig. 3c) and trilayer PP/PE/PP (Fig. 3d) separators. Their morphologies largely result from how they are manufactured (wet stretching of PE, dry stretching of PP, dry stretching of PP and double-sided ceramic coating, and dry stretching of PP/PE/PP), as exemplified by the fact that even separators of the same material can have distinct structures. For example, the PE separator in Fig. 1c exhibits a fibrous structure from a wet-casting process, while the flattened compact structure of Fig. 3a stems from a wet-stretching process. However, even though the top views of these two separators look different, their cross-sections exhibit similar isotropic features. This is in contrast to the anisotropy of the PE layer visible in the cross-section of the multilayer separator (Fig. 3d). These SEM images highlight that two-dimensional (2D) imaging is not sufficient to capture the complexity of the 3D pore network.

The earliest attempts at visualizing separator microstructure used transmission electron microscopy (TEM)[47]. For example, the anisotropic structure of a PP separator was qualitatively described by infilling the separator structure, staining the infilling phase and then carrying out SEM and TEM on the microtomed slices[48].

To quantify the structure of a porous membrane, one ideally needs a 3D representation of the structure that is sufficiently large to be reflective of the separator as a whole and of sufficient resolution to contain all key structural features. In polyolefin separators, both the pore structure and polymer backbone are on the length scale of tens of nanometres, although the nanofibres that extend across the larger pores in PP separators can be even smaller[47,48]. Scale-space analysis, in which the size of the image domain is systematically varied and the spread in microstructural parameters is analysed, indicates that, in the case of an isotropic PE separator, for example, a volume of 2 μm^3 is sufficient to capture the average properties of the separator[20].

These spatial constraints (resolution and image size) mean that both electron and X-ray-based imaging can be applied. While X-ray tomographic imaging has the advantage of being non-destructive, it offers lower resolution than focused-ion beam (FIB) SEM tomography. To date, FIB-SEM tomography[20,40] has been performed on PE and PP separators with a voxel size of 10 nm, and X-ray phase contrast tomography[39] has been carried out on PP and PP/PE/PP separators with a 63.1 nm voxel size and on a ceramic-coated PE separator with a 126.2 nm voxel size. For both techniques, sample preparation presents a challenge.

In the case of FIB-SEM analysis, polyolefins are non-conductive and therefore subject to sample charging. This has been solved by sputter coating the sample with, for example, Au/Pd or Pt of several nanometres thickness. Furthermore, pore-edge contrast and backplane information of the pore space prevents accurate binarization of the imaged dataset into pore and polymer phase. Quantitative and accurate binarization therefore requires a smooth surface and sufficient contrast between the pore and polymer phase; this has been achieved, for example, by infilling the pore phase with butter and staining the butter with osmium tetroxide[20].

With accurate 3D representations, like those provided open source[49,50], a variety of volumetric and directional microstructural parameters can be calculated. Porosity, ε, can be determined from open (that is, connected pore space) and closed (that is, disconnected pore space) volumes. Steady-state Fickian numerical diffusion simulations can be used to extract the directional tortuosity, τ, and effective transport coefficient, δ, by calculating D_{eff} and comparing it with the diffusivity of the bulk electrolyte (D_{el}): $\delta = \varepsilon/\tau = D_{eff}/D_{el}$. Such simulations yield the geometrically effective transport parameter, $\delta_{geo,eff}$, which describes how ionic transport is impacted by structure and does not include the effect of interfacial interactions between electrolyte and separator surface (Fig. 2). Numerical flow simulations can be used to extract the directional permeability, κ. These calculations can be carried out using open-source and

Table 2 | Selected separator characterization techniques with examples for extracted parameters

	Type of analysis	Parameters extracted
Imaging techniques	**Tomographic analysis**	
	•FIB-SEM tomography	Morphology •Porosity •Tortuosity •Pore dimensions
	•X-ray phase contrast tomography	Morphology •Porosity •Tortuosity •Pore dimensions
Non-imaging techniques	**Electrochemical analysis**	
	•Linear sweep voltammetry and cyclic voltammetry	Electrochemical stability
	•Electrochemical impedance spectroscopy	MacMullin number via bulk electrolyte conductivity σ and effective electrolyte conductivity σ_{sep}
	•Potentiostatic polarization combined with electrochemical impedance spectroscopy	Lithium-ion transference number according to Bruce–Vincent method[97]
	Spectroscopic and diffractive methods	
	•NMR	Transport properties •Diffusion coefficients •Conductivity •Transference number
	•X-ray diffraction	Structural composition •Degree of crystallinity
	Thermomechanical analysis	
	•Compressive loading	Effective membrane moduli •Young's modulus •Flow stress
	•Thermo-gravimetric analysis and differential scanning calorimetry	Brittleness and stability •Ductile-to-brittle transition temperature •Melting temperature
	Surface analysis	
	•BET analysis	Pore characteristics •Specific surface area •Pore radii
	•Wetting analysis	Electrolyte affinity •Contact angle •Electrolyte uptake
		Wicking behaviour •Wicking speed •Electrolyte capacity

Measured and calculated values for specific separators for each characterization technique are shown in Supplementary Table 1.

commercial codes, such as PuMA by NASA[51], TauFactor written in MATLAB by Cooper et al.[52] and GeoDict by Math2Market.

Other physical methods for characterizing structure include air permeability measurements, mercury porosimetry and Brunauer–Emmett–Teller (BET) measurements. Air permeability measurements, often referred to as Gurley measurements[53], have been used to gain insights into transport properties. Variations in air permeability have been linked to uneven current densities and degradation effects in separators. However, such measurements can be unreliable as they do not consider Knudsen-type interactions of the gas molecules with the pore walls that occur for pore diameters comparable to the mean free diffusion path of air molecules[53]. Mercury porosimetry[54] has been used to measure pore structure dimensions as well as changes in pore characteristics induced by aging[55]; although the structure-relevant results are ultimately based on SEM imaging. Specific surface area and average pore diameter have also been measured by BET[56], though measurement data for the same separator can differ by an order of magnitude (see Supplementary Table 1). A summary of methods for measuring pore size distributions in membranes is given in ref. [57].

Separator surface–electrolyte interactions. To describe the interaction between electrolyte and separator surface, one can measure the contact angle and surface tension[58]. Alternatively, in an approach adopted from the textile industry, recent work has shown that wetting can be characterized by measuring the wicking speed and the electrolyte capacity for a given separator/electrolyte pairing[24].

A separator's good electrolyte wettability also correlates with good transport performance. Numerous studies on surface-modified PE and PP separators (that is, coated with metal oxide or ceramic nanoparticles[59], plasma treated[60,61], modified with ultrathin polyelectrolyte layers[62], and coated or gelled with micrometre-thick layers of ion-conducting polymers[63]) indicate improvements in both electrolyte uptake and ionic transport. Even when such coatings decrease porosity or increase tortuosity, improvements in both σ_{eff} and t_+ are still to be observed, because the surface modifications

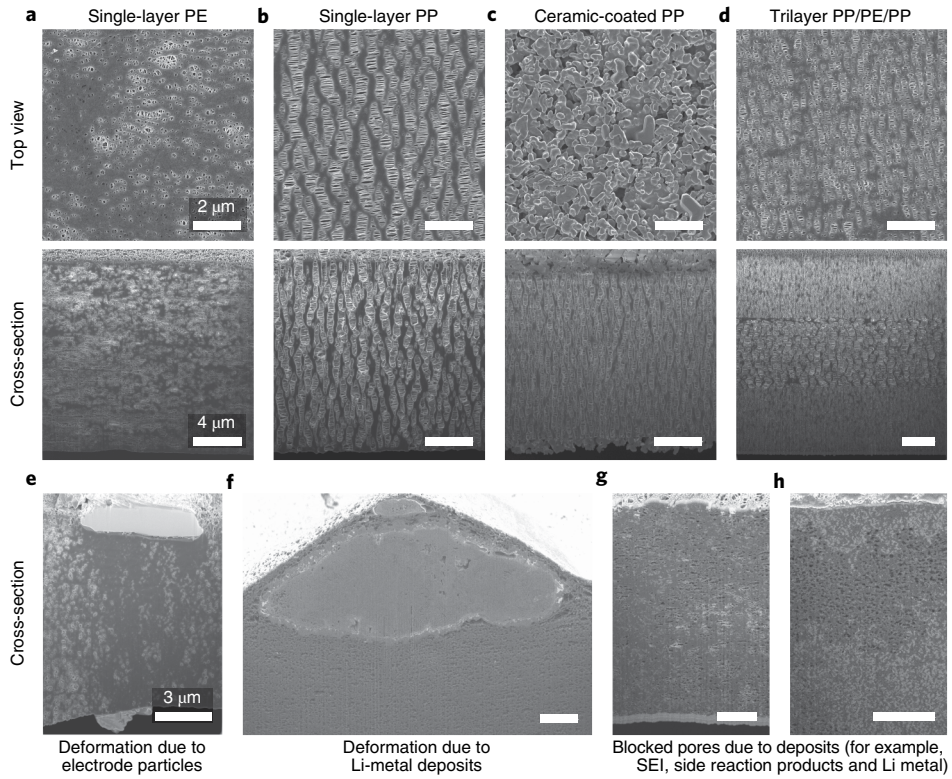

Fig. 3 | Separator structure and degradation. a–d, Surface (top) and cross-section (bottom) scanning electron micrographs of PE (**a**), PP (**b**), ceramic-coated PP (**c**) and trilayer PP/PE/PP (**d**) separators. **e**,**f**, Deformation of PE separator due to electrode particles (**e**) and Li-metal deposits (**f**). **g**,**h**, Blocked PE separator pores due to deposits (for example, SEI, side reaction products, Li metal). Panels adapted from: **a**,**b**,**f**,**h**, ref. [20], ECS; **e**,**g**, ref. [46], ECS.

locally change the solvation of the Li^+ ions or the interaction with the electrolyte's anions or cations.

Therefore, transport measurements can be used to extract information about surface–electrolyte interactions. The effective transport coefficient, δ_{eff}, is commonly determined by measuring the ionic conductivity of Li^+ ions in the electrolyte across the separator (σ_{eff}) using electrochemical impedance spectroscopy[64]. Knowing σ_{el}, the ionic conductivity of the bulk electrolyte, one can calculate δ_{eff} (or the MacMullin number N_M, which is often used in separator literature[65]) according to $\delta_{eff} = 1/N_M = \varepsilon/\tau = \sigma_{eff}/\sigma_{el}$. The effective transport coefficient, δ_{eff}, can also be determined by measuring the diffusion coefficients of lithium ions in the separator and in the bulk electrolyte. The effective diffusion coefficients can be deduced from relaxation experiments in a two-electrode (Li versus Li) cell using a porous separator[66,67] or directly measured by nuclear magnetic resonance. The second approach has been used extensively[43,44], and results show that the ion mobility in separators is influenced not only by the structure of the pore space but also by specific molecular interactions.

The measured effective transport parameter, δ_{eff}, often differs from the geometrically effective transport parameter, $\delta_{geo,eff}$, calculated using diffusion simulations on 3D reconstructions. These differences have been linked to electrolyte separator interactions[45]. The discrepancy between experimentally derived electrochemical measurements and the results of diffusion simulations makes it challenging to reliably quantify surface–electrolyte interactions. For example, unfavourable surface–electrolyte interactions will result in poor electrolyte uptake, resulting in empty pores and blocked-off transport pathways and leading to an artificially low value of measured conductivity[68]. Geometrical specifics of the pore network may also cause electrochemical and diffusion-based simulations to differ[45,69].

Impact of cell dynamics on separator performance. In the discussion above, we treated the separator as a static component. In fact, mechanical, thermal and electrochemical effects occurring in the lithium-ion cell have an ongoing impact on the separator. The separator structure, its chemical composition and the electrolyte composition all impact how a separator will respond to the dynamic processes occurring in a cell. As summarized in Table 2, many properties that influence the dynamic behaviour of separators have been experimentally measured (see Supplementary Table 1).

Important mechanical properties[70] include Young's modulus and the flow stress, which can be deduced from the strain rate-dependent stress–strain curves. While tensile properties are relevant in manufacturing, they are poor at predicting the amount of compressive stress a separator may experience during cell cycling[27]. Models to analyse stresses in the separator due to (de)lithiation and different winding geometries have been developed[71,72], and the impact of local pore closure on lithium plating has been examined[73], which can occur in response to pressure from active materials[46]. In investigating the mechanical properties of separators, computational studies have proved particularly useful. For the typical stresses found in lithium-ion cells, mostly elastic behaviour is expected; locally, however, plastic deformation can occur[33,46] due to electrode particles (Fig. 3e) and Li-metal deposits (Fig. 3f). Compressive stress leads to porosity reduction as described with a three-stage pore-collapse relation[74]. The impact of unidirectional compressive stress on separator microstructure and separator electrochemical performance has been calculated, and it was further found that both the structure of the separator and the viscoelastic properties of the separator play a role in determining the extent of strain that a separator experiences in response to a given stress[46].

Many of these studies on the mechanical properties of a separator highlight that a separator immersed in an electrolyte will have

different mechanical properties from a dry separator, and that the extent of the difference is dependent on the electrolyte solvent[25,38,75]. This is described by the Flory–Huggins interaction parameter, χ, which can be calculated using molecular dynamics simulations[76] and estimated with the Universal Quasichemical Functional-group Activity Coefficients Free Volume model (UNIFAC-FV)[25]. While the effect of mechanical softening can be determined with tensile and compressive experiments[25,26], the extent of separator swelling has not yet been quantified, and qualitative imaging of the surface and of cross-sections does not indicate significant changes in volume or features. Swelling behaviour is also complex. In semi-crystalline polyolefin separators such as PP, only the amorphous regions swell and soften, but not the crystalline regions[76].

As the typical operating temperature for a cell is in the range of 0–45 °C, and cells operating at room temperature can heat internally by many degrees Celsius during fast charge and discharge due to resistive losses in the cell[77], the thermal properties of separators (for example, heat shrinkage, thermal softening, melting) are also important in understanding how lithium-ion transport will be affected within the cell. PP and PE have fairly comparable properties[78], except for their ductile-to-brittle transition temperatures (T_g = 10 °C for PP and T_g = −120 °C for PE), and that separators made of the same material vary due to differences in polymer molecular weight, degree of crystallinity and processing conditions. The polymer can yield to mechanical load only above T_g. Since 10 °C is well within the operating range, PE might be a more suitable choice as a separator material than PP. In contrast to mechanical properties that differ between dry and wet separators, the thermal properties (for example, shrinkage) are not reported to deviate significantly. In both cases, the relative shrinkage is under 5% below 100 °C (ref. [79]). Significant differences in thermal properties can be achieved in separators that include ceramic coatings. They are generally more heat resistant[80] and exhibit low shrinking (<1% shrinkage below 150 °C)[81]. SEM observations reveal that polyolefin separators are impaired by a reduction in pore length and partial clogging caused by thermal aging; this may lead to reduced effective conductivity and transport parameters[55].

Finally, electrochemical degradation processes in separators are still an open topic of research that will undoubtedly benefit from advances in characterization and simulation. One study has used phase field simulations on dendrite–separator interactions[82] and found that dendrite penetration into the separator can be suppressed by the right selection of pore size, pore spacing and angle of inclination of pore channels, again highlighting the important role of structure in addition to chemistry in the performance and safety of lithium-ion batteries. Recent experimental and simulation work[83] demonstrates that the size and shape of separator inhomogeneities influences the prevalence and severity of localized Li plating at graphite anodes. Both FIB-SEM[20] and X-ray phase contrast tomography[84] have been used to visualize the morphology of Li deposits in symmetric Li versus Li or half-cells across separators, and the evolution of Li microstructures and deposits in LIB separators that can (partially) block (Fig. 3g,h), deform (Fig. 3f) and rupture separators.

In summary, due to the complex phenomena and dynamic processes occurring in LIB operation and the challenges associated with visualizing them dynamically (particularly in the case of highly localized, small-length-scale effects), accurate 3D representations and simulations of separator structure will become increasingly important.

Conclusions and outlook

Separators may not be electrochemically active materials, but they are far from being passive components. Both the separator structure and the interaction between pore-space surface and liquid electrolyte impact Li^+-ion transport and contribute to cell overpotentials.

Despite the expected shift away from liquid electrolytes and separator membranes and towards solid electrolytes, polyolefin separators and liquid electrolytes will likely be around for many years to come due to the challenges still facing solid electrolytes and lithium-metal anodes[85,86] and the many pathways for optimizing separator and liquid electrolytes technology. The difficulties associated with achieving low impedance interfaces in all solid-state technology as well as the importance of separator–electrolyte interactions in existing technology also highlights, for example, the promise of intermediate solutions such as gel electrolytes[63,87], which are separators that trap large amounts of liquid electrolyte in their polymer matrix and thus combine characteristics of both liquid electrolytes and solid electrolytes.

Innovation in separator technology — guided by experimental characterization, simulation and analysis — is needed to ensure that separators evolve with lithium-ion technology that is placing new demands on separators and electrolytes[13,88]. These advances include, for example, higher charge and discharge rates enabled by new electrode design and additives[89], higher capacity cells achieved with thick electrodes or new active materials (such as alloying or conversion anodes or high voltage cathodes) and longer cycle-life expectations for cells[90,91].

We predict that this innovation in separator technology will take the form of a transition from separators as passive battery elements to separators as active components, engineered for their structural and chemical properties. Separator selection will turn into separator design, with separators becoming incorporated into cells as highly customized components designed to work with specific cell chemistries and for specific applications (for example, power versus energy). This has indeed already been partly realized by using task-specific surface functionalization and coatings of polyolefin separators to prevent shuttling of polysulfides and poisoning of the electrode in Li-S batteries[92,93], and to improve SEI growth for Li-metal anodes[94]. Material composition of the separator will branch out to new polymeric materials such as polyetherimide as well as to a broad variety of Li^+-ion conducting membranes (for example, polymer–ceramic composites and non-oxide- and oxide-based inorganic materials)[95]. With time, we expect separators to be viewed as a continuation of the electrodes themselves (perhaps even directly coated on them) with both structural and chemical functionality in mind.

The transition of separators to custom-designed components that will vary for different cell chemistries and designs and that will add new function into cells will require characterization techniques that are generalizable to a wide-range of separator chemistries and task-specific surface functionalizations.

For the moment, to begin this move towards customization of separators, accurate representations of current separator structure in combination with experimental studies and simulations of the mechanical, thermal and electrochemical dynamics in cells are needed to extend our current understanding of separator operation and the ability of separators to influence and benefit cell performance. We must develop models that move beyond the homogenized picture of separator operation, and that include local effects such as structural inhomogeneities, deformation or heterogeneous ageing. Finding suitable models that describe the implications of these parameters on separator performance or that characterize the ability of a separator to mitigate these effects will be fundamental in guiding separator development. This calls for an interdisciplinary approach, with inspiration to be drawn from the analysis and design of porous media and network structures in numerous other fields, including soil physics, natural and artificial biological structures (for example, bone), and information and communication science.

Received: 8 June 2017; Accepted: 2 November 2018;
Published online: 31 December 2018

References

1. Palacín, M. R. & De Guibert, A. Why do batteries fail? *Science* **351**, 1253292 (2016).
2. Arora, P. & Zhang, Z. Battery separators. *Chem. Rev.* **104**, 4419–4462 (2004).
3. Lee, H., Yanilmaz, M., Toprakci, O., Fu, K. & Zhang, X. A review of recent developments in membrane separators for rechargeable lithium-ion batteries. *Energy Environ. Sci.* **7**, 3857–3886 (2014).
   A review describing lithium-ion battery separator types, manufacturing routes and separator performance.
4. Deimede, V. & Elmasides, C. Separators for lithium-ion batteries: a review on the production processes and recent developments. *Energy Technol.* **3**, 453–468 (2015).
5. Zhang, H., Zhou, M.-Y., Lin, C.-E. & Zhu, B.-K. Progress in polymeric separators for lithium ion batteries. *RSC Adv.* **5**, 89848–89860 (2015).
6. Nunes-Pereira, J., Costa, C. M. & Lanceros-Méndez, S. Polymer composites and blends for battery separators: state of the art, challenges and future trends. *J. Power Sources* **281**, 378–398 (2015).
7. Pintauro, P. N. Perspectives on membranes and separators for electrochemical energy conversion and storage devices. *Polym. Rev.* **55**, 201–207 (2015).
8. Chandrasekaran, R. Quantification of contributions to the cell overpotential during galvanostatic discharge of a lithium-ion cell. *J. Power Sources* **262**, 501–513 (2014).
9. Müller, S. et al. Quantifying inhomogeneity of lithium ion battery electrodes and its influence on electrochemical performance. *J. Electrochem. Soc.* **165**, A339–A344 (2018).
10. Bandhauer, T. M., Garimella, S. & Fuller, T. F. A critical review of thermal issues in lithium-ion batteries. *J. Electrochem. Soc.* **158**, R1–R25 (2011).
11. Liu, Q. Q., Petibon, R., Du, C. Y. & Dahn, J. R. Effects of electrolyte additives and solvents on unwanted lithium plating in lithium-ion cells. *J. Electrochem. Soc.* **164**, A1173–A1183 (2017).
12. Valøen, L. O. & Reimers, J. N. Transport properties of $LiPF_6$-based Li-ion battery electrolytes. *J. Electrochem. Soc.* **152**, A882–A891 (2005).
13. Erickson, E. M. et al. Review-development of advanced rechargeable batteries: a continuous challenge in the choice of suitable electrolyte solutions. *J. Electrochem. Soc.* **162**, A2424–A2438 (2015).
14. Doyle, M., Fuller, T. F. & Newman, J. The importance of the lithium ion transference number in lithium/polymer cells. *Electrochim. Acta* **39**, 2073–2081 (1994).
15. Zugmann, S. et al. Measurement of transference numbers for lithium ion electrolytes via four different methods, a comparative study. *Electrochim. Acta* **56**, 3926–3933 (2011).
16. Gores, H. J. et al. in *Handbook of Battery Materials* (eds Daniel, C. & Besenhard, J. O.) 525–626 (Wiley-VCH Verlag, Weinheim, 2011).
17. Djian, D., Alloin, F., Martinet, S., Lignier, H. & Sanchez, J. Y. Lithium-ion batteries with high charge rate capacity: influence of the porous separator. *J. Power Sources* **172**, 416–421 (2007).
18. Harris, S. J. & Lu, P. Effects of inhomogeneities — nanoscale to mesoscale — on the durability of Li-ion batteries. *J. Phys. Chem. C* **117**, 6481–6492 (2013).
19. Ramadass, P., Haran, B., White, R. & Popov, B. N. Capacity fade of Sony 18650 cells cycled at elevated temperatures: Part II. Capacity fade analysis. *J. Power Sources* **112**, 614–620 (2002).
20. Lagadec, M. F., Ebner, M., Zahn, R. & Wood, V. Communication — Technique for visualization and quantification of lithium-ion battery separator microstructure. *J. Electrochem. Soc.* **163**, A992–A994 (2016).
21. Cannarella, J. et al. Mechanical properties of a battery separator under compression and tension. *J. Electrochem. Soc.* **161**, F3117–F3122 (2014).
    Compression experiments and simulations of separators; systematic analysis of strain rate-dependent mechanical properties of dry and immersed separators.
22. Cannarella, J. & Arnold, C. B. The effects of defects on localized plating in lithium-ion batteries. *J. Electrochem. Soc.* **162**, A1365–A1373 (2015).
23. Wood, D. L., Li, J. & Daniel, C. Prospects for reducing the processing cost of lithium ion batteries. *J. Power Sources* **275**, 234–242 (2015).
24. l'Abee, R., DaRosa, F., Armstrong, M. J., Hantel, M. M. & Mourzagh, D. High temperature stable Li-ion battery separators based on polyetherimides with improved electrolyte compatibility. *J. Power Sources* **345**, 202–211 (2017).
25. Gor, G. Y., Cannarella, J., Leng, C. Z., Vishnyakov, A. & Arnold, C. B. Swelling and softening of lithium-ion battery separators in electrolyte solvents. *J. Power Sources* **294**, 167–172 (2015).
26. Xu, J., Wang, L., Guan, J. & Yin, S. Coupled effect of strain rate and solvent on dynamic mechanical behaviors of separators in lithium ion batteries. *Mater. Des.* **95**, 319–328 (2016).
27. Cannarella, J. & Arnold, C. B. Stress evolution and capacity fade in constrained lithium-ion pouch cells. *J. Power Sources* **245**, 745–751 (2014).
28. Barai, A. et al. The effect of external compressive loads on the cycle lifetime of lithium-ion pouch cells. *J. Energy Storage* **13**, 211–219 (2017).
29. Xu, J. et al. Deformation and failure characteristics of four types of lithium-ion battery separators. *J. Power Sources* **196**, 137–145 (2016).
30. Peabody, C. & Arnold, C. B. The role of mechanically induced separator creep in lithium-ion battery capacity fade. *J. Power Sources* **196**, 8147–8153 (2011).
31. Orendorff, C. J. The role of separators in lithium ion cell safety. *Electrochem. Soc. Interface* **21**, 61–65 (2012).
32. Chandrasekaran, R. Quantification of bottlenecks to fast charging of lithium-ion-insertion cells for electric vehicles. *J. Power Sources* **271**, 622–632 (2014).
33. Bach, T. C. et al. Nonlinear aging of cylindrical lithium-ion cells linked to heterogeneous compression. *J. Energy Storage* **5**, 212–223 (2016).
34. Ecker, M., Shafiei Sabet, P. & Sauer, D. U. Influence of operational condition on lithium plating for commercial lithium-ion batteries — electrochemical experiments and post-mortem-analysis. *Appl. Energy* **206**, 934–946 (2017).
35. Zhang, X., Zhu, J. & Sahraei, E. Degradation of battery separators under charge–discharge cycles. *RSC Adv.* **7**, 56099–56107 (2017).
36. Whitaker, S. Flow in porous media I: a theoretical derivation of Darcy's law. *Transp. Porous Media* **1**, 3–25 (1986).
37. Torquato, S. *Random Heterogeneous Materials* (Springer Science+Business Media, New York, 2002).
38. Gor, G. Y., Cannarella, J., Prevost, J. H. & Arnold, C. B. A model for the behavior of battery separators in compression at different strain/charge rates. *J. Electrochem. Soc.* **161**, F3065–F3071 (2014).
39. Finegan, D. P. et al. Characterising the structural properties of polymer separators for lithium-ion batteries in 3D using phase contrast X-ray microscopy. *J. Power Sources* **333**, 184–192 (2016).
40. Lagadec, M. F., Zahn, R., Müller, S. & Wood, V. Topological and network analysis of lithium ion battery components: the importance of pore space connectivity for cell operation. *Energy Environ. Sci.* **11**, 3194–3200 (2018).
    Transport simulations for different separator pore structures demonstrate the importance of non-traditional network parameters for describing separator performance.
41. Müllner, T., Unger, K. K. & Tallarek, U. Characterization of microscopic disorder in reconstructed porous materials and assessment of mass transport-relevant structural descriptors. *New J. Chem.* **40**, 3993–4015 (2016).
42. Gering, K. L. Prediction of electrolyte conductivity: results from a generalized molecular model based on ion solvation and a chemical physics framework. *Electrochim. Acta* **225**, 175–189 (2017).
43. Saito, Y., Morimura, W., Kuratani, R. & Nishikawa, S. Factors controlling the ionic mobility of lithium electrolyte solutions in separator membranes. *J. Phys. Chem. C* **120**, 3619–3624 (2016).
    NMR measurements of diffusion coefficients of ions and solvent molecules in separator pores; discussion of how ion diffusion and electrolyte properties are influenced by separator geometry and surface interactions.
44. Saito, Y., Morimura, W., Kuse, S., Kuratani, R. & Nishikawa, S. Influence of the morphological characteristics of separator membranes on ionic mobility in lithium secondary batteries. *J. Phys. Chem. C* **121**, 2512–2520 (2017).
45. Zahn, R., Lagadec, M. F., Hess, M. & Wood, V. Improving ionic conductivity and lithium-ion transference number in lithium-ion battery separators. *ACS Appl. Mater. Interfaces* **8**, 32637–32642 (2016).
46. Lagadec, M. F., Zahn, R. & Wood, V. Designing polyolefin separators to minimize the impact of local compressive stresses on lithium ion battery performance. *J. Electrochem. Soc.* **165**, A1829–A1836 (2018).
47. Bierenbaum, H. S., Isaacson, R. B., Druin, M. L. & Plovan, S. G. Microporous polymeric films. *Ind. Eng. Chem. Prod. Res. Dev.* **13**, 2–9 (1974).
48. Sarada, T., Sawyer, L. C. & Ostler, M. I. Three dimensional structure of Celgard microporous membranes. *J. Memb. Sci.* **15**, 97–113 (1983).
    Visualization of the three-dimensional microstructure of polypropylene separators using electron microscopy.
49. Lagadec, M. F., Ebner, M. & Wood, V. *Microstructure of Targray PE16A Lithium-Ion Battery Separator* (ETH Zurich, 2016); https://doi.org/10.5905/ethz-1007-32
50. Lagadec, M. F. & Wood, V. *Microstructure of Celgard PP1615 Lithium-Ion Battery Separator* (ETH Zurich, 2018); https://doi.org/10.3929/ethz-b-000265085
51. Ferguson, J. C., Panerai, F., Borner, A. & Mansour, N. N. PuMA: the porous microstructure analysis software. *SoftwareX* **7**, 81–87 (2018).
52. Cooper, S. J., Bertei, A., Shearing, P. R., Kilner, J. A. & Brandon, N. P. TauFactor: an open-source application for calculating tortuosity factors from tomographic data. *SoftwareX* **5**, 203–210 (2016).
53. Hantel, M. M., Armstrong, M. J., DaRosa, F. & l'Abee, R. Characterization of tortuosity in polyetherimide membranes based on Gurley and electrochemical impedance spectroscopy. *J. Electrochem. Soc.* **164**, A334–A339 (2017).
54. Abraham, K. M. & Alamgir, M. Polymer electrolytes reinforced by Celgard membranes. *J. Electrochem. Soc.* **142**, 683–687 (1995).
55. Martinez-Cisneros, C., Antonelli, C., Levenfeld, B., Varez, A. & Sanchez, J. Y. Evaluation of polyolefin-based macroporous separators for high temperature Li-ion batteries. *Electrochim. Acta* **216**, 68–78 (2016).
56. Song, J. Y., Wang, Y. Y. & Wan, C. C. Conductivity study of porous plasticized polymer electrolytes based on poly(vinylidene fluoride): a comparison with polypropylene separators. *J. Electrochem. Soc.* **147**, 3219–3225 (2000).

57. Tung, K. L. et al. Recent advances in the characterization of membrane morphology. *Curr. Opin. Chem. Eng.* **4**, 121–127 (2014).
58. Dahbi, M. et al. Interfacial properties of LiTFSI and $LiPF_6$-based electrolytes in binary and ternary mixtures of alkylcarbonates on graphite electrodes and Celgard separator. *Ind. Eng. Chem. Res.* **51**, 5240–5245 (2012).
59. Cheng, Q., He, W., Zhang, X., Li, M. & Song, X. Recent advances in composite membranes modified with inorganic nanoparticles for high-performance lithium ion batteries. *RSC Adv.* **6**, 10250–10265 (2016).
60. Huang, C., Lin, C. C., Tsai, C. Y. & Juang, R. S. Tailoring surface properties of polymeric separators for lithium-ion batteries by cyclonic atmospheric-pressure plasma. *Plasma Process. Polym.* **10**, 407–415 (2013).
61. Li, B. et al. Facile and nonradiation pretreated membrane as a high conductive separator for Li-ion batteries. *ACS Appl. Mater. Interfaces* **7**, 20184–20189 (2015).
62. Xu, W. et al. Layer-by-layer deposition of organic-inorganic hybrid multilayer on microporous polyethylene separator to enhance the electrochemical performance of lithium-ion battery. *ACS Appl. Mater. Interfaces* **7**, 20678–20686 (2015).
63. Stephan, A. M. Review on gel polymer electrolytes for lithium batteries. *Eur. Polym. J.* **42**, 21–42 (2006).
64. Landesfeind, J., Hattendorff, J., Ehrl, A., Wall, W. A. & Gasteiger, H. A. Tortuosity determination of battery electrodes and separators by impedance spectroscopy. *J. Electrochem. Soc.* **163**, A1373–A1387 (2016).
65. Huang, X. Separator technologies for lithium-ion batteries. *J. Solid State Electrochem.* **15**, 649–662 (2011).
66. Thorat, I. V. et al. Quantifying tortuosity in porous Li-ion battery materials. *J. Power Sources* **188**, 592–600 (2009).
67. Ehrl, A., Landesfeind, J., Wall, W. A. & Gasteiger, H. A. Determination of transport parameters in liquid binary electrolytes: I. Diffusion coefficient. *J. Electrochem. Soc.* **164**, A826–A836 (2017).
68. Devaux, D. et al. Conductivity of carbonate- and perfluoropolyether-based electrolytes in porous separators. *J. Power Sources* **323**, 158–165 (2016).
69. Zahn, R., Lagadec, M. F. & Wood, V. Transport in lithium ion batteries: reconciling impedance and structural analysis. *ACS Energy Lett.* **2**, 2452–2453 (2017).
70. Plaimer, M. et al. Evaluating the trade-off between mechanical and electrochemical performance of separators for lithium-ion batteries: methodology and application. *J. Power Sources* **306**, 702–710 (2016).
71. Xiao, X., Wu, W. & Huang, X. A multi-scale approach for the stress analysis of polymeric separators in a lithium-ion battery. *J. Power Sources* **195**, 7649–7660 (2010).
72. Shi, D., Xiao, X., Huang, X. & Kia, H. Modeling stresses in the separator of a pouch lithium-ion cell. *J. Power Sources* **196**, 8129–8139 (2011).
73. Cannarella, J. & Arnold, C. B. The effects of defects on localized plating in lithium-ion batteries. *J. Electrochem. Soc.* **162**, A1365–A1373 (2015).
74. Pan, Y. & Zhong, Z. Modeling the ion transport restriction in mechanically strained separator membranes. *J. Electrochem. Soc.* **161**, A583–A586 (2014).
75. Sheidaei, A., Xiao, X., Huang, X. & Hitt, J. Mechanical behavior of a battery separator in electrolyte solutions. *J. Power Sources* **196**, 8728–8734 (2011).
76. Yan, S., Xiao, X., Huang, X., Li, X. & Qi, Y. Unveiling the environment-dependent mechanical properties of porous polypropylene separators. *Polymer* **55**, 6282–6292 (2014).
77. Forgez, C., Vinh Do, D., Friedrich, G., Morcrette, M. & Delacourt, C. Thermal modeling of a cylindrical $LiFePO_4$/graphite lithium-ion battery. *J. Power Sources* **195**, 2961–2968 (2010).
78. Love, C. T. Perspective on the mechanical interaction between lithium dendrites and polymer separators at low temperature. *J. Electrochem. Energy Convers. Storage* **13**, 031004 (2016).
Analysis of the temperature- and shape-dependent mechanical interactions between lithium dendrites and separators.
79. *Development of an Advanced Microporous Separator for Lithium Ion Batteries Used in Vehicle Applications* (United States Advanced Battery Consortium, 2018).
80. Xu, H., Zhu, M., Marcicki, J. & Yang, X. G. Mechanical modeling of battery separator based on microstructure image analysis and stochastic characterization. *J. Power Sources* **345**, 137–145 (2017).
81. Dai, J. et al. A rational design of separator with substantially enhanced thermal features for lithium-ion batteries by the polydopamine–ceramic composite modification of polyolefin membranes. *Energy Environ. Sci.* **9**, 3252–3261 (2016).
82. Jana, A., Ely, D. R. & García, R. E. Dendrite–separator interactions in lithium-based batteries. *J. Power Sources* **275**, 912–921 (2015).
83. Liu, X. M., Fang, A., Haataja, M. P. & Arnold, C. B. Size dependence of transport non-uniformities on localized plating in lithium-ion batteries. *J. Electrochem. Soc.* **165**, 1147–1155 (2018).
Experimental and theoretical analysis of how structural separator inhomogeneities affect ion transport.
84. Sun, F. et al. Morphological evolution of electrochemically plated/stripped lithium microstructures investigated by synchrotron X-ray phase contrast tomography. *ACS Nano* **10**, 7990–7997 (2016).
85. Kerman, K., Luntz, A., Viswanathan, V., Chiang, Y.-M. & Chen, Z. Practical challenges hindering the development of solid state Li ion batteries. *J. Electrochem. Soc.* **164**, A1731–A1744 (2017).
86. Xu, C., Ahmad, Z., Aryanfar, A., Viswanathan, V. & Greer, J. R. Enhanced strength and temperature dependence of mechanical properties of Li at small scales and its implications for Li metal anodes. *Proc. Natl Acad. Sci. USA* **114**, 57–61 (2017).
87. Hallinan, D. T. & Balsara, N. P. Polymer electrolytes. *Annu. Rev. Mater. Res.* **43**, 503–525 (2013).
88. Feng, X. et al. Thermal runaway mechanism of lithium ion battery for electric vehicles: a review. *Energy Storage Mater.* **10**, 246–267 (2018).
89. Etacheri, V., Marom, R., Elazari, R., Salitra, G. & Aurbach, D. Challenges in the development of advanced Li-ion batteries: a review. *Energy Environ. Sci.* **4**, 3243–3262 (2011).
90. Nitta, N., Wu, F., Lee, J. T. & Yushin, G. Li-ion battery materials: present and future. *Mater. Today* **18**, 252–264 (2015).
91. Hassoun, J. & Scrosati, B. Advances in anode and electrolyte materials for the progress of lithium-ion and beyond lithium-ion batteries. *J. Electrochem. Soc.* **162**, A2582–A2588 (2015).
92. Bauer, I., Thieme, S., Brückner, J., Althues, H. & Kaskel, S. Reduced polysulfide shuttle in lithium-sulfur batteries using Nafion-based separators. *J. Power Sources* **251**, 417–422 (2014).
93. Zhu, W. et al. Improving the electrochemical performance of polypropylene separator through instantaneous photo-induced functionalization. *J. Electrochem. Soc.* **165**, A1909–A1914 (2018).
94. Ryou, M. H. et al. Excellent cycle life of lithium-metal anodes in lithium-ion batteries with mussel-inspired polydopamine-coated separators. *Adv. Energy Mater.* **2**, 645–650 (2012).
95. Sun, Y. Lithium ion conducting membranes for lithium-air batteries. *Nano Energy* **2**, 801–816 (2013).
96. Kirchhöfer, M., Von Zamory, J., Paillard, E. & Passerini, S. Separators for Li-ion and Li-metal battery including ionic liquid based electrolytes based on the TFSI- and FSI- anions. *Int. J. Mol. Sci.* **15**, 14868–14890 (2014).
97. Bruce, P. G. & Vincent, C. A. Steady state current flow in solid binary electrolyte cells. *J. Electroanal. Chem.* **225**, 1–17 (1987).
98. Wood, V. X-ray tomography for battery research and development. *Nat. Rev. Mater.* **3**, 293–295 (2018).

Acknowledgements

The authors gratefully acknowledge support from an ETH research grant (0-20978-14) and the European Research Council (project 680070).

Author contributions

All authors contributed to developing and writing the manuscript.

Competing interests

The authors declare no competing interests.

Additional information

Supplementary information is available for this paper at https://doi.org/10.1038/s41560-018-0295-9.

Reprints and permissions information is available at www.nature.com/reprints.

Correspondence should be addressed to V.W.

Publisher's note: Springer Nature remains neutral with regard to jurisdictional claims in published maps and institutional affiliations.